FINITE ELEMENT TRANSIENT THERMAL ANALYSIS OF AN AXIALLY SPLIT HORIZONTAL MULTISTAGE PUMP

by

Roland Kaiser

Senior Design Engineer-Analyst

Sulzer Bingham Pumps

Portland, Oregon

Wolfram Lienau

Senior Development Engineer

Sulzer Innotec AG

Winterthur, Switzerland

and

Douglas Peters

Technical Director

Renaissance Design Inc.

Portland, Oregon

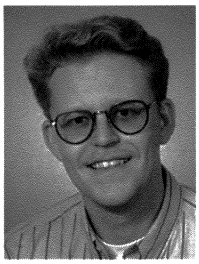

Roland Kaiser is a Senior Design Engineer-Analyst with Sulzer Bingham Pumps, in Portland, Oregon. He joined the Acoustic & Vibration Department of Sulzer Innotec in 1987, and took on activities in the areas of active noise suppression and vibration analysis and testing. In 1990, he joined the Mechanical Development Group of Sulzer Pumps Headquarters. His activities included vibration analysis of pump rotors and structures. Mr. Kaiser was involved in multiphase pump development and testing, which included product lubricated bearings. He developed and validated computer codes used to simulate rotordynamic behavior with experimental data of annular seal configurations, typically used in the pump industry. In 1994, he joined Sulzer Bingham Pumps and took on responsibilities for new product development. His activities also include testing and simulation of new products.

Mr. Kaiser studied at Engineering College (HTL) in Winterthur, Switzerland, where he graduated with a diploma in Mechanical Engineering.

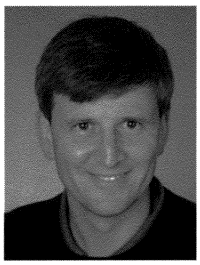

Wolfram Lienau is a Senior Development Engineer with Sulzer Innotec AG in Winterthur, Switzerland. After three years working as a teaching assistant at the technical university in Darmstadt, Germany, he joined the R&D division of Eastman Christensen, a drilling equipment producer located in Celle, Germany. Mr. Lienau's activities included the strength calculation of drilling tools, components of them, and the mechanical behavior of drill pipes, mainly by means of finite element analyses. In 1990, he joined Sulzer Innotec as the head of the Structural Mechanics Group. Sulzer Innotec supports the product divisions of the Sulzer technology corporation, as well as external customers, with engineering services and R&D projects.

Mr. Lienau studied at the Mechanical University Braunschweig, in Germany, where he received his master diploma (Mechanical Engineering). He is registered at NAFEMS as a finite element analyst at the advanced level.

Douglas Peters is the Technical Director for Renaissance Design Inc., in Portland, Oregon, and has been using high-end CAD software to create complex designs and design engines for the past 11 years. After joining the then startup RDI in New Hampshire, in 1988, he moved on to start successful offices for RDI in Michigan, in 1990, and in Oregon, in 1995. Mr. Peters and RDI provide on and offsite design and engineering CAD services using Pro/Engineer and Unigraphics, specializing in complex freeform objects and robust associative parametric modelling. Currently, he is heading "design engine" projects where very robust models and assemblies allow many designs or design iterations to be created, checked to existing standards, and automatically detailed very quickly.

Mr. Peters received his B.S. degree (Mechanical Engineering) from Rensselaer Polytechnic Institute.

ABSTRACT

Often the industrial power generation market specifies that boiler feedpumps must be capable of withstanding thermal transient conditions when operating in boiler feed service. A thermal transient analysis was performed in order to better define whether an axial split multistage pump design was suitable for service conditions specified for the combined cycle power market.

The pump is a nonsymmetric design and contains complex hydraulic shapes that required 3-D modelling to accurately represent the real geometric conditions. The analysis model was built using currently available 3-D CAD technology.

Once developed, the 3-D model was translated into finite element (FE) code by international graphics exchange standard (IGES) translation. The 3-D model was then further divided into smaller portions to allow meshing. The model was meshed with 407,000 elements with 541,000 nodes, which resulted in 1.8 million degrees of freedom (Figure 1).

Figure 1. Finite Element Mesh—Cut Up.

INTRODUCTION

The finite element model selected for the 3-D analysis is an eight stage, axially split, between bearings, multistage horizontal pump. The pump is approximately 2.4 meters long with a power input of 1270 kW. A pump of this size is typically rated at 300 m^3/h to 400 m^3/h (1300 gpm to 1800 gpm) at a discharge head of between 1082 m to 1265 m (3550 ft to 4150 ft) at 3575 rpm. The casing material is chrome steel ASTM A487 grade CA6NM. Stationary rings are chrome steel at 400HB to 450HB and the shaft is type 410 chrome steel. Gasket material is typically synthetic fiber plus binder with a thickness of 1/64 of an inch.

The purpose of this analysis was to verify, and improve if necessary, the design of boiler feedpumps and to simplify their starting procedure in thermal peak-load plants. The thermal loads created through faster starting were simulated, and the behavior of individual pump components investigated, under different thermal simulated conditions. Answers to the following questions were sought during the analysis:

- Does the pump meet the specified thermal loads?
- Under which thermal load could pump damage due to metal-to-metal contact or due to overstressed regions occur (e.g., thermal stress, excess displacement, or distortion of casing or internal components, etc.)?
- How can these effects be mitigated?

Special consideration was to be given to the behavior of the gasket and bolt loads, as this may indicate conditions under which the case leaks. The other prime consideration was whether the rotor makes contact with the casing, which would indicate a potential for usually destructive rubbing between rotor and stationary parts.

The axially split pump consists of a lower and upper casing half, which are bolted together. Since the lower casing half contains the suction and discharge nozzle, it is more complicated than the upper half. An additional aspect for consideration is the fact that the wall thickness varies continuously due to the complexity of the hydraulic channels. The impellers in this pump are arranged in an opposed manner and therefore subject the bearings to low axial loads. In this eight-stage pump, the pumpage is routed through channel crossovers to the pump end opposite the suction flange after the fourth stage.

Finite element technology allows simulation of pump casing behavior under various transient and steady-state conditions (e.g., hydropressure, operating pressure, and thermal transients). It was expected that the finite element model would be extremely large with regard to number of elements, and prior to this investigation, there was limited experience available with such large analysis models.

The main purpose of the investigation was to verify whether the existing pump design can be subjected to a higher thermal transient and thermal shock than previously established. This pump model has existing limits on thermal loading of 5°F/min for the ramp and 100°F for thermal shock. The industrial power generation market requires up to 18°F/min heatup rate and 150°F instantaneous thermal shock.

Different load cases, including bolt pretension, hydropressure, operating pressure, thermal ramp of 20°F/min up and down, and thermal shock of 200°F up and down, were analyzed. For those load cases, the Von Mises stresses have been evaluated, as well as casing displacements in general. To help ensure casing closure integrity, special consideration has been given to gasket compression and residual bolt pretension for each bolt. Pump operability is further checked by gauging the difference in the distortion of the case bores to the pump rotor radial growth, to evaluate the pump running clearances.

Improvements were found that can be made to the existing design to reduce overall displacement values. Case bore distortions have been evaluated with consideration to wear ring growth and shaft growth. The resulting running clearances are only relevant to the warm-up transients, since under cool-down transients the clearances tend to increase. Resulting clearances at the most critical point in time for each warm-up load case are evaluated.

3-D CAD SOLID MODEL

A solid model of the pump was created using the Unigraphics CAD modelling package. Model geometry is reflective of the pump design—no simplifying assumptions were made (Figure 2).

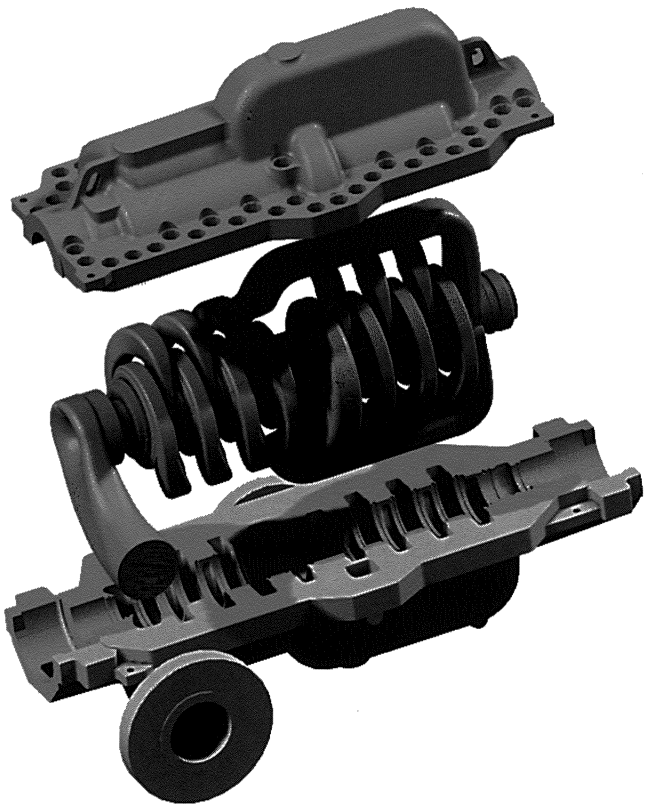

Figure 2. 3-D CAD Model—Pump Assembly.

To speed modelling and software performance, each individual component of the pump, such as the long crossover, short crossover, suction, discharge, and case features, was built in a

separate file. This also allowed some parts to be built in parallel, further speeding the modelling process. Each of these parts is fully parametric, allowing changes with a minimum of rework.

Highly complex hydraulic shapes were constructed with parametric curves in the proper position. These surfaces were then used to trim the solid created earlier by extrusion of sketched curves. Then various variable-radius blends are added to complete the hydraulic component. Because of the construction method, parts of each body can be changed or recreated easily without recreating the entire model. This means that changes can be more quickly investigated and that the model can be used as a template for other pumps in the future, without starting from scratch.

The final pump model is formed by assembling the component solids together. A mathematical expression controls the length of the long crossover, the number and positions of the short crossovers, the position of the suction and discharge, and position and configuration of mounting flanges and holes. The flange, boss, and hydraulic wall thickness solids are united, and then the hydraulic and hole solids are subtracted. Finally all blends (at transitions) are applied. By changing the stage expression, the entire pump can be changed to a four, five, six, seven, or eight stage pump.

The 3-D CAD geometry was exported to ANSYS (finite element analysis tool) via the IGES interface, where the solid model had to be reworked extensively because volumes are not supported by IGES and some surfaces were not trimmed correctly (Figure 3).

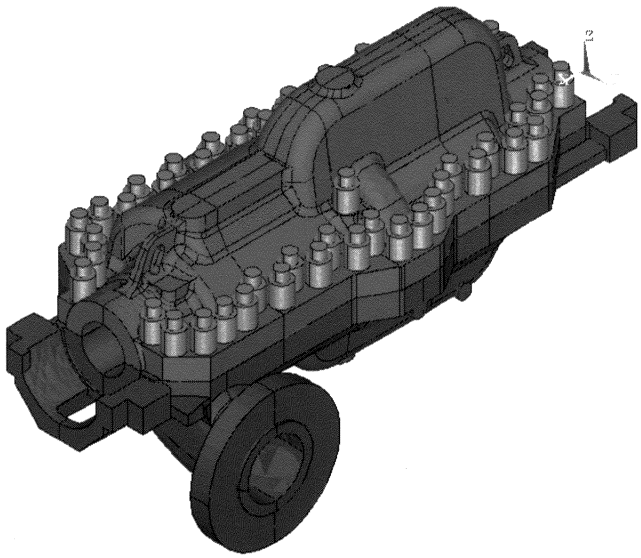

Figure 3. Solid Model.

Hidden errors in CAD model files represent a major hurdle for the finite element analysis process. The analyst usually has to perform "cleanup" work first, before analysis work can actually commence. Typical was the evidence of small gaps that are difficult to find visually on screen, and slivers that are small elongated faces that are generated to patch between larger surfaces in a model. All those problems had to be corrected. Model tuning and corrections were done within the finite element program. It would not have been efficient to rework the 3D CAD model again. The types of problems encountered with this project at the next phase involved matching of part geometries—typical for such a complex model. For all the advances in finite element analysis (FEA) technology, it is important to remind the reader that model creation and debugging still require significant input and time from the analyst.

To accommodate the FEA model meshing, the upper half of the casing was divided into eight volumes, and the more complicated lower half, with both suction and discharge nozzle, was divided into nine volumes. Additional volumes were created for each of the 51 bolts and the thin gasket.

FINITE ELEMENT MODEL—CASING

The pump casing for the static calculations was meshed with 10-node tetrahedrons within ANSYS, producing some 407,000 elements (Figure 1). The element size was 20 mm (0.785 inch). This was the coarsest mesh that could be generated with this geometry. Some interior walls of the structure were meshed with only one element over their thickness. Bolts and gasket were meshed with eight node hexahedrons. Dissimilar nonmatching meshes were used for all parts, and the meshes were "glued" together using tied contact that cannot separate, or, alternatively, between the gasket and the upper flange side of the casing, using real contact conditions. For this contact description, a small sliding formulation was used making the calculations nonlinear.

Because of memory allocation limitations and the advantages (outlined below) of using ABAQUS (finite element analysis tool) against ANSYS, the decision was made to convert the finite element model into ABAQUS for the analysis part only. The FE model was translated into the ABAQUS input format by means of an "inhouse" interface program.

For the analyses, ABAQUS Version 5.6 was chosen due to the following reasons:

- Pretension bolt loading can be applied to all bolts simultaneously.
- Sparse solver, dramatically saving disk space, memory, and CPU-time
- Modified second order tetrahedrons for contact
- Contact definition with dissimilar meshes and element types
- Robustness, especially for contact analyses
- No limitations in model size
- Interpolation of nodal temperature values to midside nodes via an external result file

To facilitate the application of pressure and heat flux loads within ABAQUS, the internal surfaces of the hydraulic channels and the seal bores were additionally meshed with overlaying thin membrane elements (Figure 4).

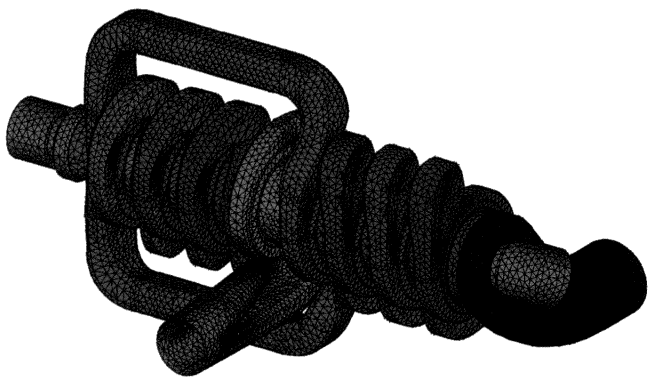

Figure 4. Finite Element Mesh—Wet Areas.

Of the 1.8 million degrees of freedom, there are the additional internal nodes of the modified tetrahedrons (Figure 5) in the flange region and the internal degrees of freedom for the contact conditions (between flange and gasket). Linear material behavior was assumed for casing, bolts, and for the gasket. Friction was neglected between the gasket and the casing to permit use of the available sparse solver. This FE model was used for the static nonlinear combined pressure and deformation analysis, due to applied selected temperature fields.

These calculations were performed on an SGI Power Challenge machine, which has 12 processors and 4 GB memory. One R10000 Processor, 700 MB of memory, and a disk capacity of 36 GB were reserved for the calculations.

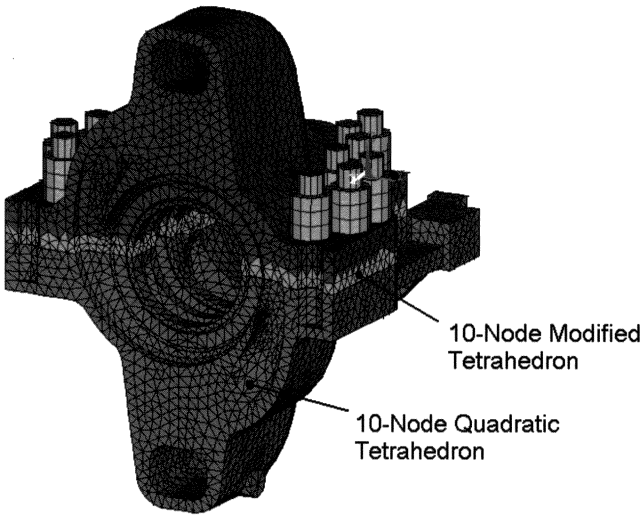

Figure 5. Element Description—Nonlinear Static Analysis.

For the thermal calculations, an alternative FE model was derived, where all the midside nodes were removed, leaving 115,000 nodes. Using this model, transient calculations were possible on a low end workstation, because each node has only one degree of freedom.

FINITE ELEMENT MODEL—ROTOR

The complete shaft assembly was modelled with the rotor wear rings and sleeves assumed to be one unit, i.e., no shrink fits between components are taken into account. Eight node structural solid 2-D plane elements were used to mesh the rotational symmetric model. The impeller vanes are considered plane stress with an equivalent thickness applied. The temperature model is meshed with equivalent eight node thermal solids.

TRANSIENT THERMAL ANALYSIS—CASING

To keep analysis times within a reasonable range, the number of load cases had to be limited. By limiting the transient thermal analysis cases to a quantity of two (20°F/min transient and 200°F instantaneous), analysis time could be kept in reasonable limits without compromising the results as these load cases are bounding. It is assumed that lesser thermal loads than those analyzed will not limit normal pump operation.

In centrifugal pumps, the fluid passes through hydraulic channels at high velocities. Therefore it is assumed that wet surface nodes will experience the bulk temperatures applied directly—film coefficients are very high and therefore not applied. Casing outside walls are assumed to be insulated—thermal radiation from the pump is not considered.

API 610 Seal Plan 23 is assumed for seal cooling, and the maximum seal flush temperature is 82°C (180°F). It is assumed that the seal bore warms up at a rate of 3.3°C/min (6.25°F/min based on the same time required to reach maximum pumpage temperature) from a starting temperature of 27°C (80°F). Cool-down rate is 1.3°C/min (2.5°F/min), to a final temperature of 60°C (140°F).

Upward Thermal Ramp

A uniform initial temperature distribution of 27°C (80°F) is applied to all nodes. Outside surfaces are at 27°C with a film coefficient of 1 W/m^2°C (0.1761 Btu/h ft^2°F)—assuming insulated conditions.

Large temperature differences between the inside of the pump and the outside of the pump will cause the highest overall deformation and stress levels. Each thermal transient was analyzed using 24 time increments. Each of those time increments had to be checked to determine the most severe case. The stress and deformation values were analyzed for only one particular point in time. The maximum temperature difference between internal and outside temperatures was reached after 16 minutes and 30 seconds, which identifies load case 1 (Figure 6). The temperature distribution for this load case is shown in Figure 7.

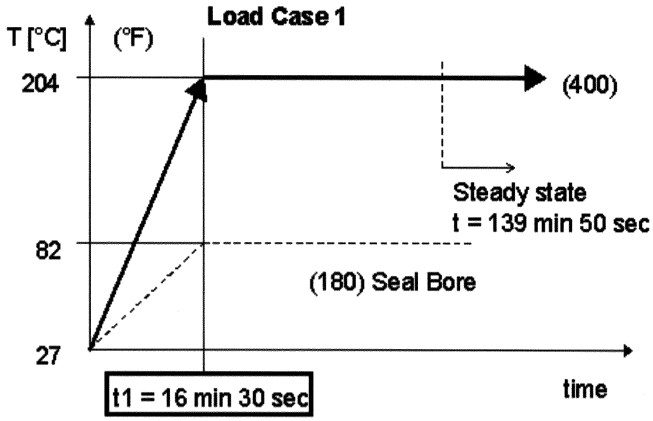

Figure 6. Applied Temperatures to Wet Areas.

Figure 7. Upward Transient, Temperature Field after t = 16 min 30 sec.

This load case is of particular interest, since it resulted in the greatest degree of closure between the pump rotor and casing, and was used in the evaluation of whether clearances were still adequate. For the warm-up, the temperatures reached steady-state conditions after 139 minutes 50 seconds.

Downward Thermal Ramp

The maximum temperature difference for the cool-down ramp is also reached after 16 minutes 30 seconds. This point in time defines thermal load case 2 (Figure 8). This load case is of interest for overall distortions, stress, and remaining gasket compression. For the cool-down, the temperatures reached steady-state conditions after 126 minutes 30 seconds.

Instantaneous Upward Thermal Shock

For this transient thermal shock load case, two time points were identified for further consideration. Load case 5 was identified to

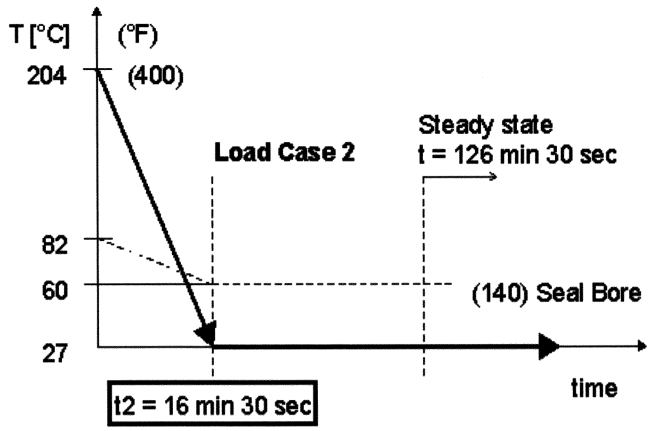

Figure 8. Applied Temperatures to Wet Areas.

be critical to remaining wear part clearances, because after 24 seconds the shaft nearly reached steady-state conditions (Figure 9). At 24 seconds, the casing outside surface is still relatively cool, restricting the growth of the casing bores. Bolt temperatures change slowly in relation to parting flange temperatures, and therefore elevated stress levels can be recognized for the bolts, improving gasket compression.

Temperature difference between bolt and pump parting flange is shown as function of time in Figure 10. This maximum temperature difference between bolt and parting flange identifies load case 3, which is after four minutes from transient initiation. This is the second point of interest for the upward thermal shock. This load case is of particular interest from the perspectives of increased bolt stress, overall case deformations, and case stress levels. Temperatures reach steady-state conditions after 92 minutes.

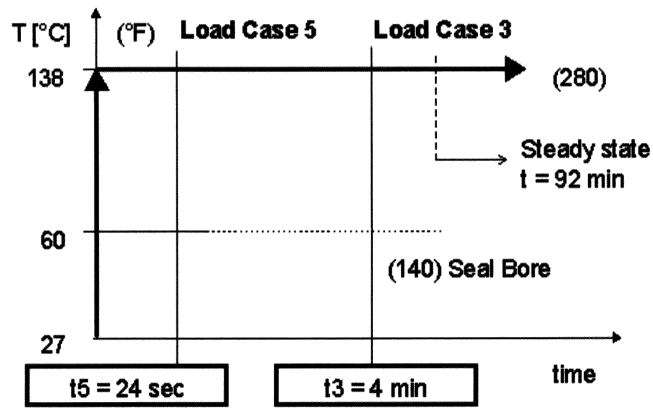

Figure 9. Applied Temperatures to Wet Areas.

Instantaneous Downward Thermal Shock

During a downward thermal transient shock, bolt pretension is reduced. This is because the bolts need more time to cool-down than does the parting flange. Therefore, gasket compression is reduced as well. This can result in leakage at the pump case splitline. Temperatures reach steady-state conditions after 78 minutes 40 seconds, according to the analysis (Figure 11).

A summary of all the thermal load cases investigated is shown in Table 1. The critical time is a point in time depicted to be used for the nonlinear analysis. The casing temperatures of these load cases will be used for the nonlinear static analysis.

TRANSIENT THERMAL ANALYSIS—ROTOR

During a plant/pump warm-up, the shaft and impellers usually expand faster than the casing. Similarly for a cool-down transient,

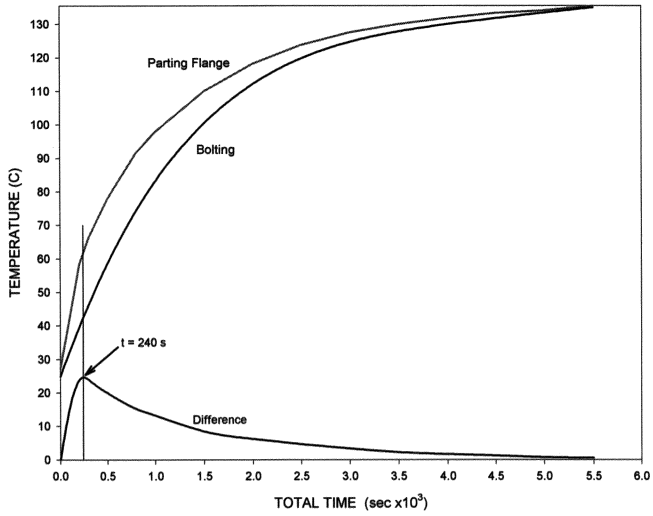

Figure 10. Temperatures as Function of Time, Bolt and Parting Flange Location.

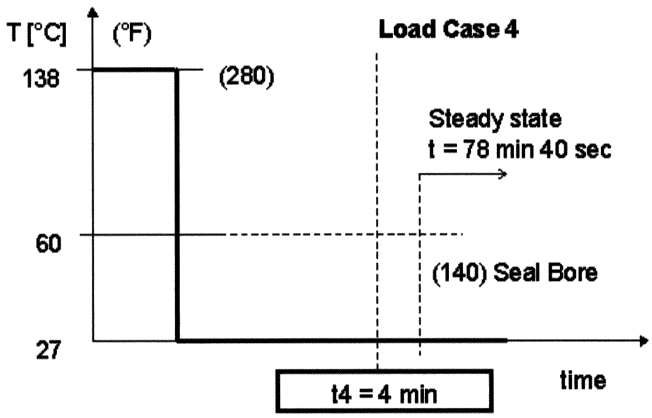

Figure 11. Applied Temperatures to Wet Areas.

Table 1. Overview of the Load Cases Analyzed.

Load Case	Description	Pumpage Start Temp.		Pumpage End Temp.		Critical Time	Steady State
		°C	°F	°C	°F	t [s]	ts [s]
1	20°F/min up	27	80	204	400	990	8390
2	20°F/min down	204	400	27	80	990	7590
3	200°F up	27	80	138	280	240	5520
4	200°F down	138	280	27	80	240	4720
5	200°F up	27	80	138	280	24	5520

the shaft and stationary rings will shrink faster than the casing. Therefore, cool-down transients should not pose any problems relative to pump internal running clearances.

The applied temperatures and film coefficients used in the analysis are shown in Tables 2 and 3. The rotating element reaches steady-state conditions after 16 minutes 30 seconds when subjected to the temperatures shown in Table 2. For the thermal shock, it takes two minutes 30 seconds to achieve steady-state conditions. The diametral growth of the rotor at eye ring and hub ring locations for each location, as well as at the throttle and center bushing locations, were entered into a database.

Table 2. Applied Bulk Temperatures and Film Coefficients, Upward Transient.

20°F / min, Up	Bulk Temperature		Film Coefficient
Location	°C	°F	W/m2K
Forced Air, Fan Cooled	27	80	100
Inside Bearing Housing	90	194	1
Bearing Sleeve	60	140	-
Seal Chamber, cooled	82	180	-
Seal Chamber, insulated	82	180	1
Pumpage	204	400	-

Table 3. Applied Bulk Temperatures and Film Coefficients, Upward Thermal Shock.

200°F, Up	Bulk Temperature		Film Coefficient
Location	°C	°F	W/m2K
Forced Air, Fan Cooled	27	80	100
Inside Bearing Housing	90	194	1
Bearing Sleeve	60	140	-
Seal Chamber, cooled	60	140	-
Seal Chamber, insulated	60	140	1
Pumpage	138	280	-

NONLINEAR STATIC ANALYSIS

The static analysis is nonlinear because of nonlinear gasket behavior. With these analyses, the deformations and stresses are calculated for all pressure and temperature combined load cases. The solutions are found iterative after solution convergence. By using gap elements for the gasket, the contact pressure on the gasket, as well as the contact pattern, can be viewed.

The two casing halves were bolted together with a gasket between them. On the top side of the gasket, surface contact was simulated, i.e., contact between two deformable bodies with a small relative motion was applied.

No additional pressure loading is taken into account for the additional casing splitline areas that are now wetted due to the parting flange opening. "Gasket opening" and "gasket compression" can be viewed in the GASKET COMPRESSION section later. The areas with low gasket compression can easily be identified on these plots. The contact surfaces between the cap nuts and top half case are not modelled with contact elements. Instead, tight contact is assumed between nut and top half. This means, that local casing surface deformations are coupled directly with the nut contact surface. Therefore, some bolts experience a significant bending stress component. Each bolt will interact with other bolts in local vicinity and therefore cause some local deformation (bending stress).

The model boundary conditions are reflective of the hot alignment procedure. One hold-down on the drive end side of the pump is restrained in all three directions, whereas the second one is only supported vertically. On the nondrive end, both feet are supported vertically, whereas one is also constrained horizontally. No nozzle loads or reactions are input into the model.

The first nonlinear static analysis run was carried out to establish proper pretension values for each bolt at room temperature. Eight iterations were necessary, using approximately 10 hours of CPU time each. Both hydrostatic proof testing pressure and pump normal operating pressure at room temperature were examined.

The temperature distribution load cases 1 through 5 (Table 1) were carried out with operating pressure loads and with the corresponding temperature distributions from the thermal transient calculation. These temperatures were stored in the result-file for each time increment during the thermal transient analysis. For the nonlinear static analysis, the nodal temperatures are applied to the main nodes directly, and for the midside nodes they are interpolated.

The combined load cases with pressure and temperature, as well as the hydropressure load case, were restarted from the first analysis case—bolt pretension analysis. All load steps converged within six to eight iterations, and the solution was stable throughout all iterations.

BOLT PRETENSION

The stud preload torque value input to the model is per pump manufacturer standard. To apply this load to the bolts in an FEA model, an iterative process is usually required, because each bolt is interacting with adjacent bolts. Usually, bolt forces must be monitored during subsequent load steps. The finite element code used for the analysis, though, utilizes an automated process available to allow the calculation of bolt pretension in one load step. Therefore, considerable analysis time could be saved during the bolt pretension load case.

In later load steps, it is the objective to allow the fastener to carry additional load. The fastener acts as a deformable component responding to other loadings in the assembly.

A bolt load of 591 kN was applied to each bolt. This bolt load equals 65 percent of the bolt yield stress at 204°C (400°F). During the different loadings of hydropressure, operating pressure, and thermal loads, the fasteners will experience additional loading to a varying degree.

As expected, hydrotest pressure loading produces the highest bolt loads. Bolt number 15 (Figure 12), which is located at the discharge volute area between stage volute #4 and #8, is loaded with 818 kN (183,886 lb), which is the maximum load. This corresponds to a normal stress of 563 N/mm^2 (81,653 psi), which equals 78 percent of yield at 20°C.

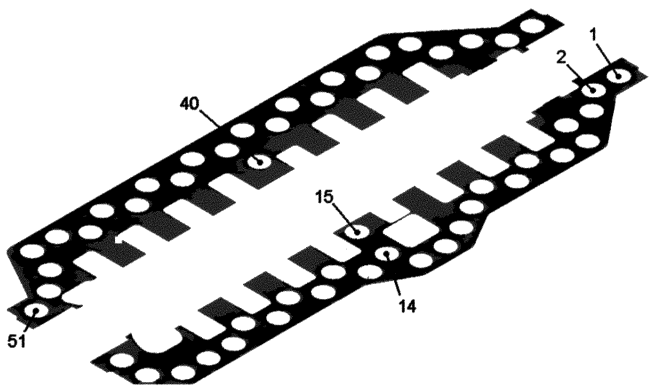

Figure 12. Bolt Location—Definition.

No bolts experience loading over the limit during simulation at hydrotest pressure. Table 4 shows the change in bolt load for some other bolt locations of interest. The change is expressed relative to the bolt pretension loads.

Each bolt location can be identified in Figure 12. Higher bolt loads can also be seen for the bolts at the mechanical seal bores. These are identified as bolt numbers 1 and 2 as well as bolt 26 and 51. It is evident that for the warm-up transients load case 1, 3, and 5, bolt loads increase. For cool-down transients load cases 2 and 4, bolt loads decrease. For bolt 15, the reduction in bolt load is 19 percent. Therefore, for cool-down transients, gasket compression is reduced.

Table 4. Relative Change in Bolt Load.

Relative change of bolt pretension in %							
Bolt Location	Test Pressure	Oper. Pressure	Thermal LC 1	Thermal LC 2	Thermal LC 3	Thermal LC 4	Thermal LC 5
1	29.4	1.7	0.9	2.1	1.6	2.6	2.4
2	20.2	1.5	3.6	1.0	3.3	1.2	2.4
14	10.4	2.7	4.9	-2.4	6.2	-2.6	5.9
15	38.3	5.0	24.2	-19.1	25.5	-18.7	19.4
26	19.4	3.4	2.9	4.4	3.6	3.8	4.4
40	23.9	2.2	26.1	-21.1	19.0	-11.5	10.0
51	6.2	1.6	4.1	-0.2	4.0	0.1	3.3

For the thermal loads investigated, bolt stresses do not reach the yield strength limit of 630 N/mm^2 (91,371 psi). Maximum bolt load during warm-up transient is 745 kN (167,476 lb), which corresponds to 81 percent of yield. In the pump industry, it is common practice to torque the bolts close to the yield strength. Increasing the bolt load by 15 percent would still be acceptable and improve gasket compression.

HYDROTEST PRESSURE

In addition to bolt pretension, uniform hydrotest pressure at room temperature was applied to all internal wet areas. For this load step, the objective was to allow the fastener to carry the additional load. Hydropressure is equivalent to 1.5 design pressure, and is 276 bar (4000 psi).

Viewing the contour plot of the Von Mises stress levels in Figure 13, the bolt locations show highest stress values. This is normal—areas of deformation appear on a frequent basis. High stress levels can also be found in the area where the long crossover intersects the boss over the first four stages. Also, the blend area around the boss shows elevated stress levels. Those stresses indicate the relatively weak areas compared with the structurally stiffer locations, and are not of concern. The area of the first four short crossovers is significantly weaker than the area where the long crossover runs over to the last four stages. Under normal operating conditions, the first four stages experience the lowest pressure. On the bottom casing half (Figure 14), elevated stress values are evident around the bolt locations and at the pump hold down locations, as expected.

Figure 13. Von Mises Stress on Top Half During Hydropressure.

Figure 15 shows the displacements of the top half case. The highest deformation values can be found on the parting flange at the discharge volute, on the suction side of the pump. The parting flange on this side deforms considerably more than on the discharge nozzle side. This difference is due mainly to the

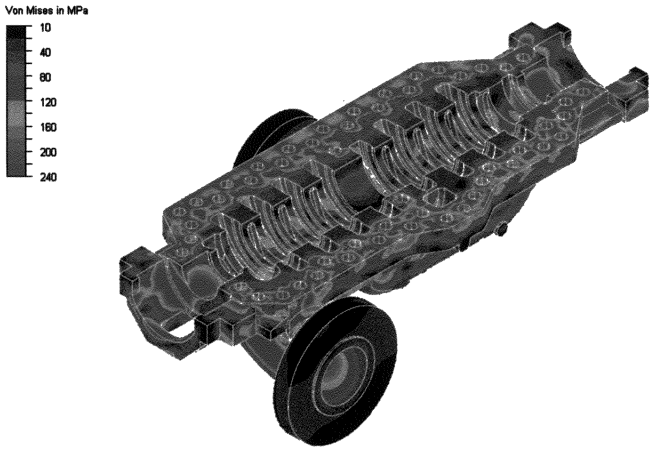

Figure 14. Von Mises Stress on Bottom Half During Hydropressure.

irregularities in the geometry. On the discharge nozzle side, the short crossover provides considerably more structural support for the parting flange than on the other side where it is unsupported.

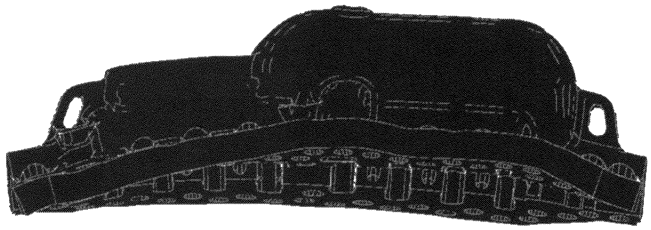

Figure 15. Deformations on Casing Top Half During Hydropressure.

Figure 16 is a cross-section through the discharge. The differences in geometry cause the structure to deform as shown. The bottom half case is very asymmetric in the area of the discharge volute and nozzle. The internal pressure in the volute acting on the structurally weaker top flange area at this location, forces the component to move in the direction of least resistance. Splitline opening in the pump is also visible on Figure 16. The opening is larger on the discharge nozzle side, since the bolts are located further away from the part centerline compared with the suction side of the pump.

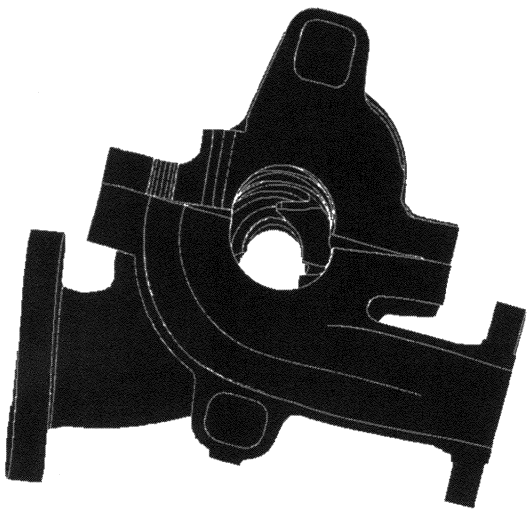

Figure 16. Deformation—Cross Section Through Discharge Nozzle During Hydropressure.

EFFECT OF OPERATING PRESSURE

In addition to bolt pretension, pressure as shown in Table 5 was applied (at room temperature) to areas of the model corresponding to actual pump operating conditions.

Table 5. The Following Stage Loading Is Applied.

Location	Pressure bar	Pressure psi
Seal bore	23.5	341
Suction	21.1	306
1st stage	36.75	533
2nd stage	53.5	776
3rd stage	70.25	1019
4th stage	87	1262
5th stage	103.75	1505
6th stage	120.5	1748
7th stage	137.25	1991
8th stage	154	2234
Discharge	154	2234

GASKET COMPRESSION

The contact pattern for each load case can be viewed on contour plots. Areas of no compression, i.e., gasket liftoff, are readily identified near the wetted portion of the pump, where compression is lost. Bolt pretension alone (Figure 17) can cause gasket liftoff at some locations. More liftoff can be seen on the discharge side. This is because the bolts are not as close to the centerline as on the opposite side. Gasket liftoff for all load cases is greater on the discharge side.

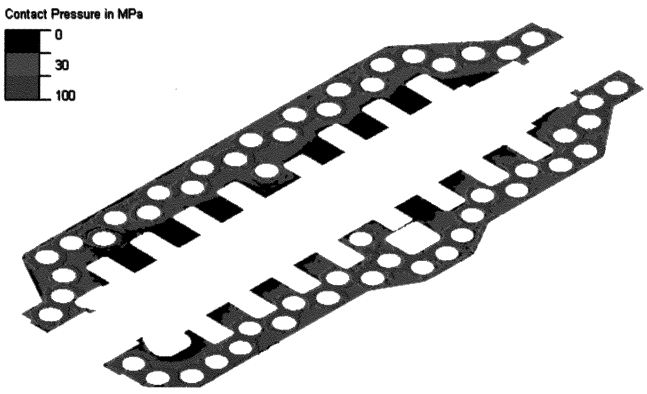

Figure 17. Gasket Compression—Bolt Pretension.

Leakage can be expected to occur through the bolt holes for hydrotest pressure load case conditions, as seen in Figure 18. Leakage through the splitline is also shown at the seal area end face on both sides. Usually during hydrostatic testing, it is a common practice to increase the torque on some of the bolts to prevent leakage. For all other load cases, no leakage is expected through the splitline, though some leakage may occur across the volutes. This is internal to the pump and is usually of no consequence.

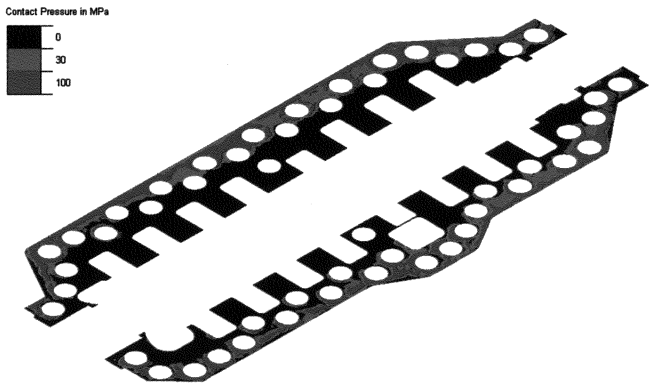

Figure 18. Gasket Compression—Hydropressure.

In general, warm-up transients result in an improved gasket contact pattern due to increased bolt loading. Conversely, cool-down transients show an increased gasket liftoff (Figure 19) due to a reduced bolt pretension. In practice, the overall leakage can be reduced by increasing bolt torque values.

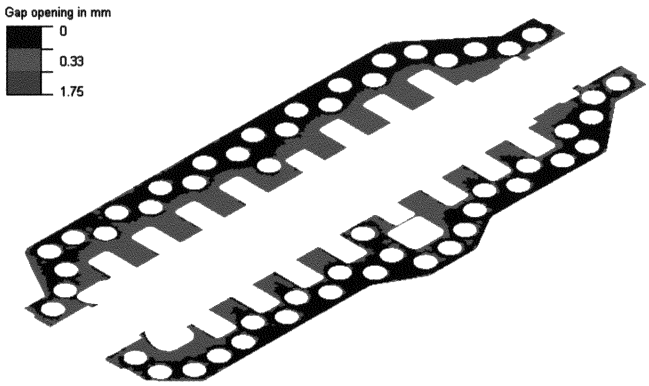

Figure 19. Gasket Opening—Cool-Down Transient with 20°F/min.

FIELD VALIDATION

It was intended to collect field data from a similar pump for validation purposes. Unfortunately, it was not possible to find a pump subjected to the same or even similar thermal conditions as were investigated. The thermal transients the pumps were subjected to in the field were about four times lower than the one analyzed. Furthermore, warm-up features were in use on those pumps. Therefore, it was decided that a comparison of calculated and measured thermal stresses could not be used for validation. However, the static loading measurements employing straingauges can be used for a straight comparison. The straingauge measurements were done on a nine stage pump, geometrically similar to the one under investigation. The following figures show temperature and strain as function of time (Figures 20, 21, and 22).

Assuming a two dimensional stress state, the Von Mises effective stress can be expressed as follows:

$$\sigma_{VM} = \sqrt{\sigma_1^2 - \sigma_1\sigma_3 + \sigma_3^2} \quad (1)$$

The strains measured are tabulated in Table 6.

The calculated Von Mises stress levels are very close to the measured levels (Figures 23 and 24). Their overall quality of the results after comparison is believed to be very close to reality. The model is therefore demonstrated to be validated.

Table 6. Comparison of Measured and Calculated Stress.

Strain Channel	Location	Stress [N/mm2]	Von Mises [N/mm2]	Calculated [N/mm2]
1 (axial)	Suction Nozzle	21	26	20-40
2 (tangential)		29.4		
3	Discharge Nozzle	42	69	NA
4		79.8		
7	Short X-Over	23.1	24	20-40
8		25.2		
9	Long X-Over	65.1	84	80-100
10		94.5		

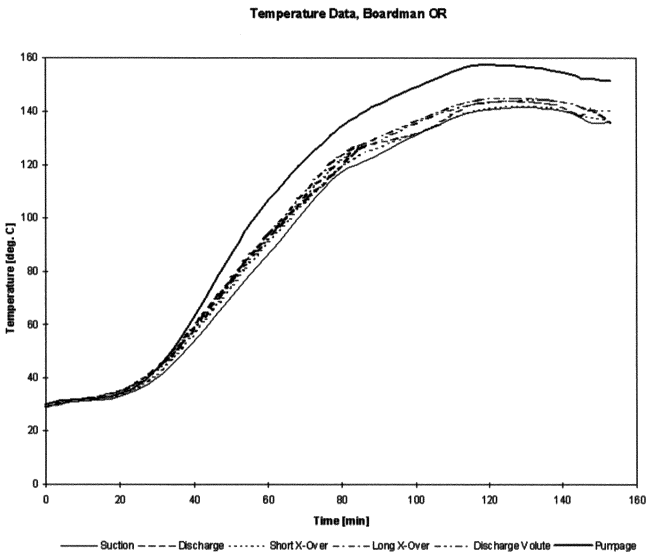

Figure 20. Housing Surface Temperatures During Thermal Transient.

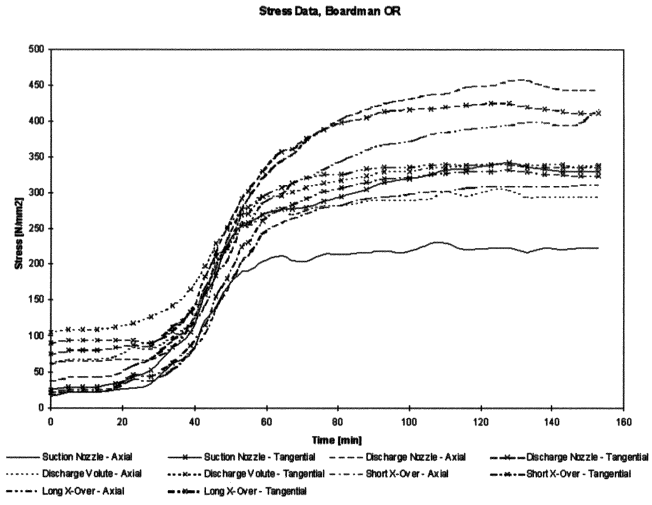

Figure 21. Measured Uncompensated Stress During Thermal Transient.

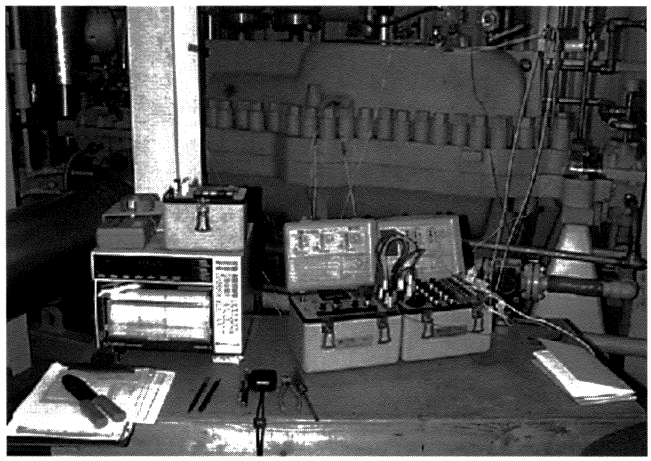

Figure 22. Test Setup on MSD 6×8×11BD 9 Stage Pump.

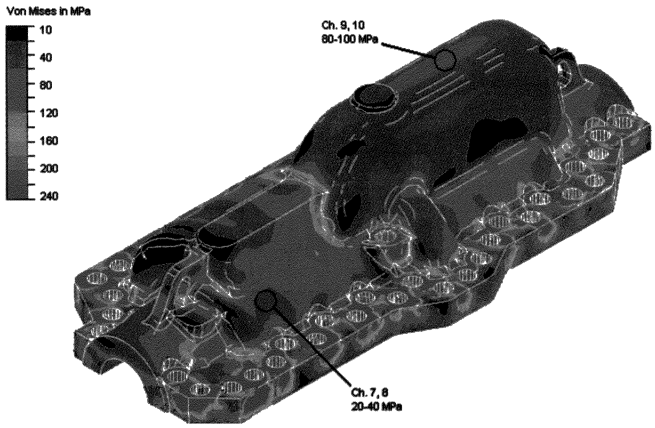

Figure 23. Top Half Von Mises Stress During Operating Pressure.

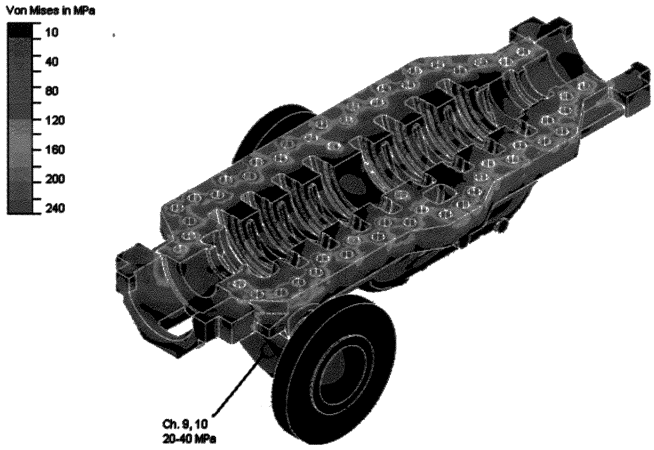

Figure 24. Bottom Half Von Mises Stress During Operating Pressure.

RIGID BODY DISPLACEMENTS

The applicable coordinate system is defined below. X-coordinate is shaft axis, starting with zero at the bearing bracket on the throttle bushing side. Figure 25 shows the finite element mesh and definitions for the pump casing bores.

When the pump is pressurized or loaded as a result of temperature change or external force acting on the casing, it distorts. All the nodes of the model experience displacements in all three directions. Consider a set of nodes defining the surface of an internal casing bore. The displacements of each node of such a bore can be visualized with a vector magnitude plot, like the one shown in Figure 26.

The mathematical average of all those displacements in each direction (horizontal and vertical) defines the amount of rigid body

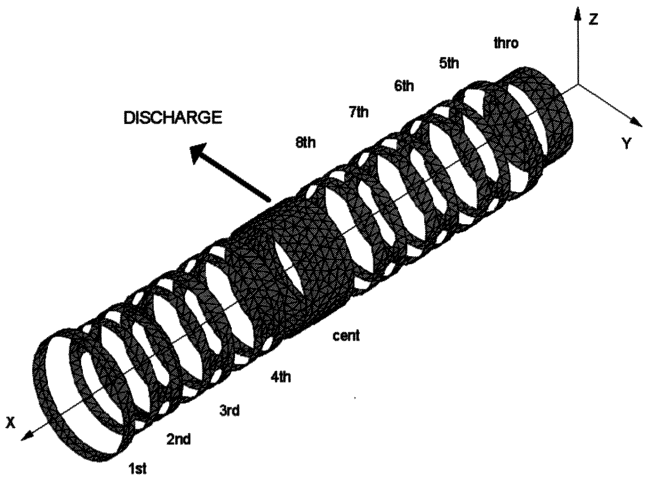

Figure 25. Definitions—Case Bore.

motion. Those displacements are shown for the two directions of interest in Figures 27 and 28 for each casing bore. Horizontal axes in the graphs defines the bore location according to the definitions in Figure 25. The coordinate system is shown in Figure 29.

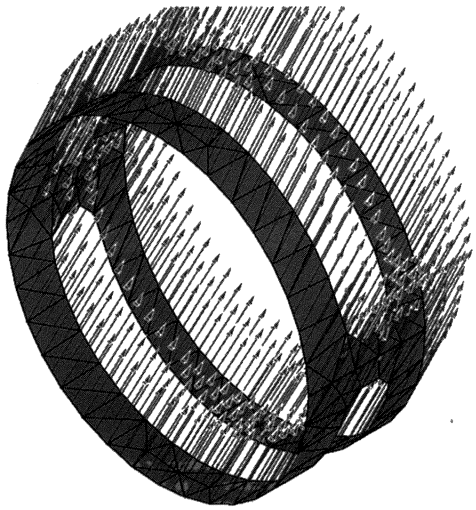

Figure 26. Case Bore—Vector Plot.

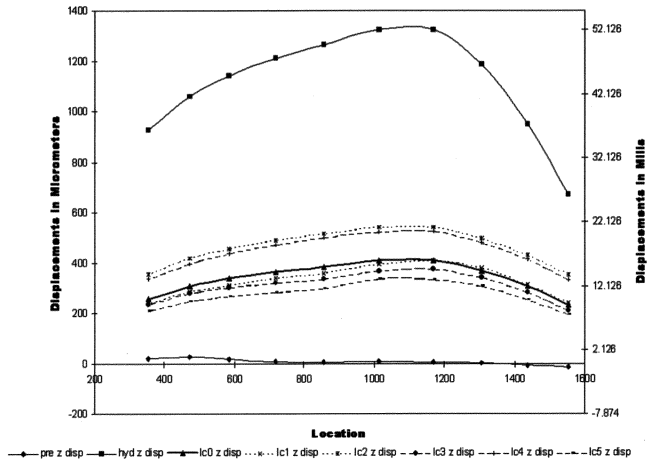

Figure 27. Vertical Rigid Body Motion (Center of Pump Machined Bores).

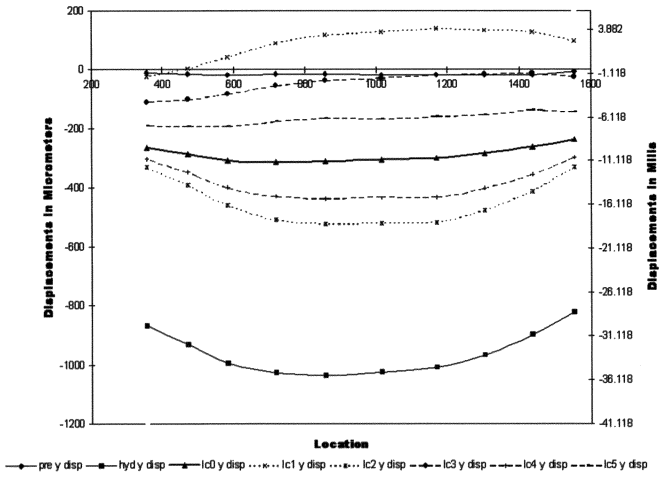

Figure 28. Horizontal Rigid Body Motion (Center of Pump Machined Bores).

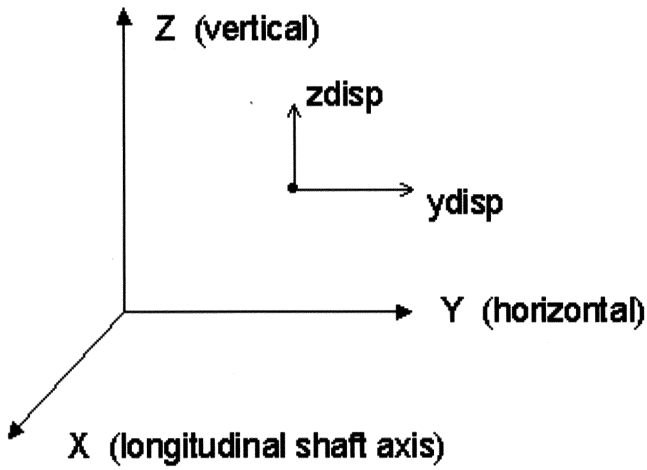

Figure 29. Coordinate System (View from First Stage, Suction).

The rigid body motion can be expressed as follows:

In the horizontal direction:

$$\text{ymove} = \frac{1}{n_{vect}} \sum_{i=1}^{n_{vect}} (\text{ydisp}) \qquad (2)$$

In the vertical direction:

$$\text{zmove} = \frac{1}{n_{vect}} \sum_{i=1}^{n_{vect}} (\text{zdisp}) \qquad (3)$$

Vertical rigid body motion of the center of the pump internal bores is shown in Figure 27, and horizontal is shown in Figure 28.

Vertical rigid body motions are defined as positive when the casing bores move up. During hydrotest pressure loading, the case deforms significantly, as seen in Figures 27 and 28. The maximum vertical bore offset is 1.3 mm for this load case.

On warm-up transients, vertical displacements tend to decrease. On cool-down transients, vertical displacements tend to increase. If put in relationship to the load case operating pressure, which assumes steady-state conditions at 27°C (80°F), casing bores move down for warm-up transients and up for cool-down transients.

During thermal transients, bore centerlines move up or down, depending on the thermal loads applied. Once the pump casing reaches steady-state temperature condition, it will assume the operating pressure displacements (at 80°F). This is true if the system behaves in a linear manner, i.e., no plastic deformation occurs.

During the warm-up transients, the horizontal displacements tend to move toward the suction nozzle. For the cool-down transients, center bores tend to move toward the discharge side. In other words, for the cool-down load cases, the displacements tend to move in the direction of increased pressure. The warm-up load cases tend to bring the bores closer to the ideal center bore locations, as during bolt pretension, without any temperature and internal pressure.

BORE DISTORTIONS

Local bore distortion was found as follows:

$$\Delta y = ydisp - ymove \quad (4)$$

$$\Delta z = zdisp - zmove \quad (5)$$

Where:

ymove = Horizontal rigid body displacement (Figure 28)
zmove = Vertical rigid body displacement (Figure 27)
ydisp = Total horizontal displacement
zdisp = Total vertical displacement

The change in bore radius can be expressed as follows:

$$\Delta R(\varphi) = \Delta y * \cos\varphi + \Delta z * \sin\varphi \quad (6)$$

The coordinate system is shown in Figure 30. The values of ΔR can be shown as function of φ for one nodal set, for all load cases in Figure 31.

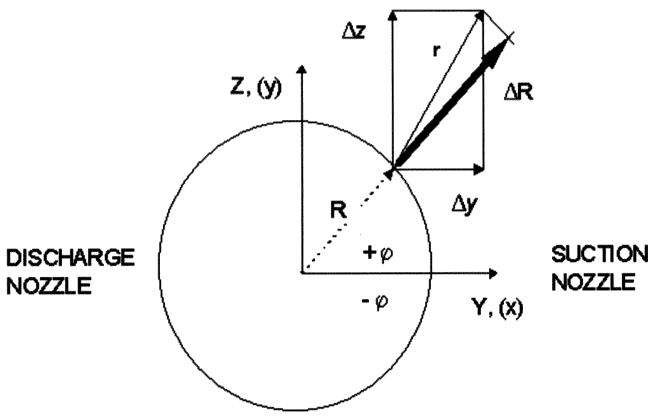

Figure 30. Coordinate System (View from First Stage, Suction).

Negative φ angles describe the bottom half of the pump casing bore, and positive angles describe the top half. Positive values of deviation mean the bore at that location is larger than the nominal value. Comparing nodal distortions 180 degrees apart, the location with the smallest diameter can be identified.

The following formula is used to present the polar plots:

$$R = 50 + \frac{1}{30} * \Delta R \quad (7)$$

The "50" circle is reference datum, i.e., undeformed bore at room temperature. According to the formula, a radial bore growth of 300 μm (11.811 mils) is represented between circles labeled "50" and "60." The "X" in the following polar plots identifies the horizontal location in meters, as defined on Figure 25.

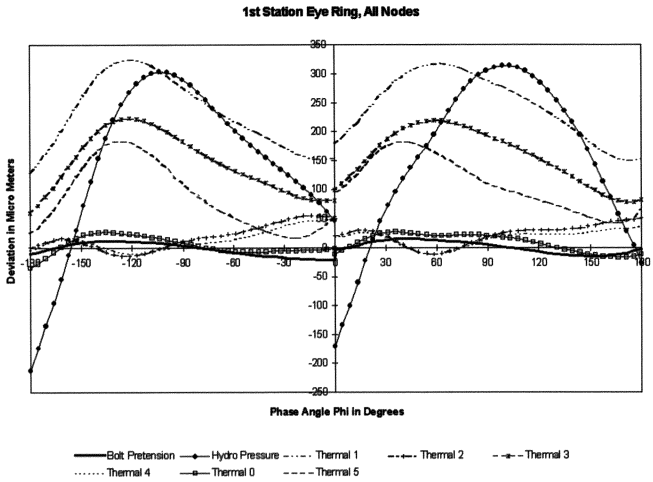

Figure 31. Bore Distortion First Stage Eye Ring.

The residual minimum bore opening for the following load cases are all at the splitline:

- Pretension
- Hydropressure
- Operating pressure
- Load case 1 (20°F/min-up)
- Load case 3 (200°F-shock-up)

For all other thermal load cases, the residual bore opening is at other locations:

- Load case 2 (20°F/min-down)
- Load case 4 (200°F-shock-down)
- Load case 5 (200°F-shock-up)

Polar plots are shown in Figures 32, 33, and 34.

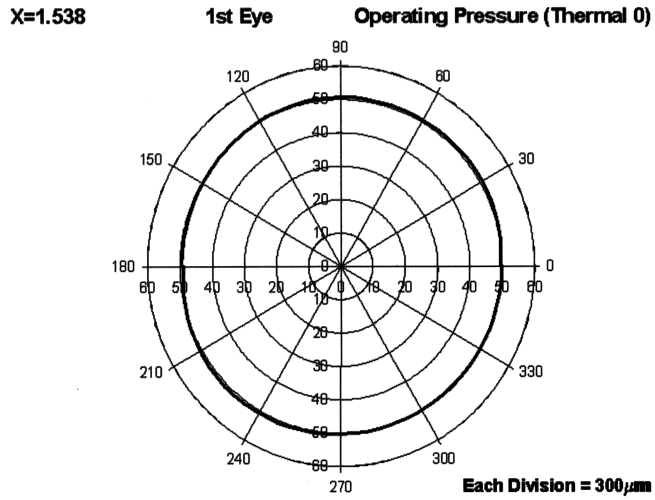

Figure 32. Polar Plot, First Eye—Operating Pressure.

REMAINING RUNNING CLEARANCES

As explained previously, only the warm-up load cases are investigated with respect to remaining clearances. The smallest case diameter will restrict further growth of the case ring. Remaining clearances are used to gauge the operability of the pump undergoing the thermal transient. The remaining running clearance can be found with the following vector diagram (Figure 35):

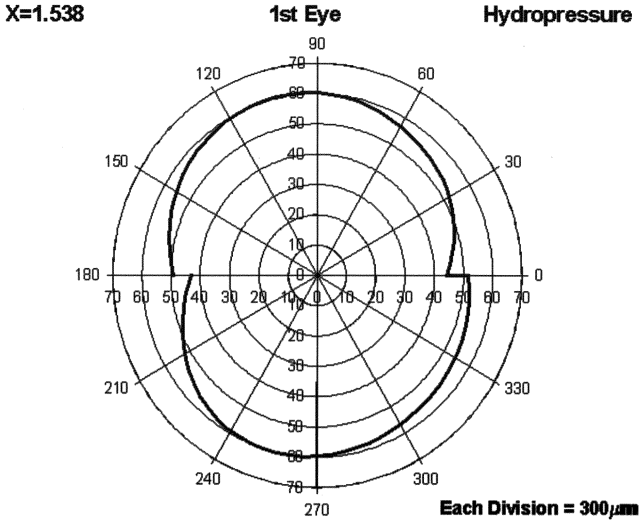

Figure 33. Polar Plot, First Eye—Hydropressure.

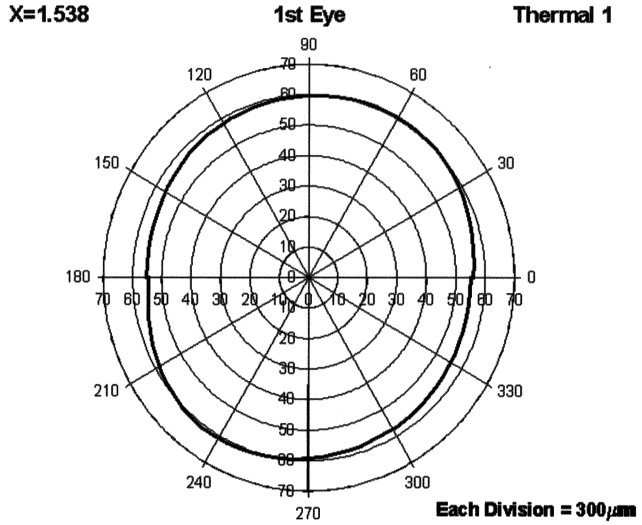

Figure 34. Polar Plot, First Eye—Thermal Load Case 1.

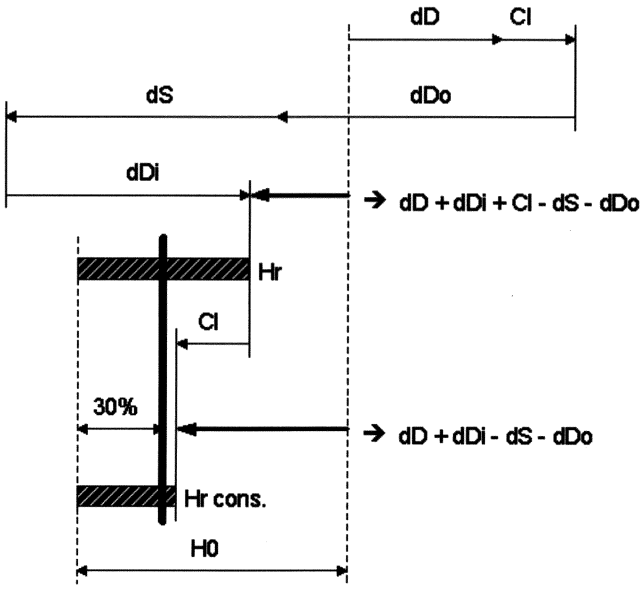

Figure 35. Clearance Vector Diagram.

Where:

H0 = Diametral running clearance
dS = Shaft
dDi = Case ring, inside
dDo = Case ring, outside
dD = Minimum case bore
Cl = Case ring clearance
Hr = Remaining running clearance

For *Hr*, it is assumed that the case ring can expand to the extent the case bore opens, plus the design clearance between case bore and ring (dD + Cl), as the case to case ring fit is normally loose.

The outer surface of the case ring is in contact with casing bore (dDo ≥ dD + Cl), and further radial growth of the inside bore of the case ring is restricted due to casing contact. It is assumed that this restriction in ring growth limits the case ring inside diameter growth to that allowed for the outside diameter (dDi – dDo + dD + Cl). It is assumed that this restriction reduces the inner diameter growth direct linear (dDi – dDo + dD + Cl).

Shaft growth will also reduce the remaining clearance. Analytically this can be written as follows:

$$Hr = H0 + dD + dDi + Cl - dS - dDo \quad (8)$$

Assuming the case rings are bound during the case growth, a more conservative approach can be offered. In the current context, the case ring is bound when the case ring is only allowed to grow as much as the case bore opens (There is no clearance between case ring and case bore.)

$$Hr\ conservative = H0 + dD + dDi - dS - dDo \quad (9)$$

The remaining clearance for each annular seal wear ring location can be shown as percentage of design running clearances. In Figures 36 and 37, percentage values are shown for eye ring locations, center and throttle bushings, for case rings bound, and not bound, respectively.

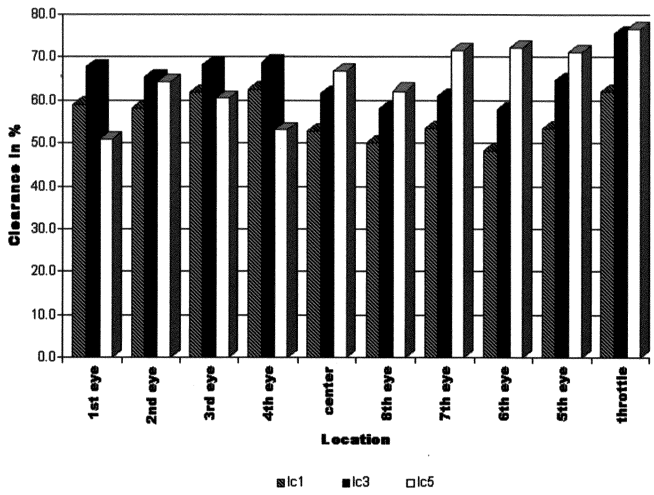

Figure 36. Remaining Clearances at Annular Seal Locations, Case Ring Not Bound.

It is believed that residual clearance of 30 percent of normal wear ring clearance is sufficient to allow the dynamic motion of the shaft, without rotor and casing contact. For the nonbound case ring example, remaining clearances are shown to be above 30 percent of nominal. For the bound case ring example, the minimum remaining clearances are between 24 percent to 40 percent of nominal design running clearance. For thermal load case 1, some of the remaining clearances dip below 30 percent. This is at center bush, eighth eye, and sixth eye location.

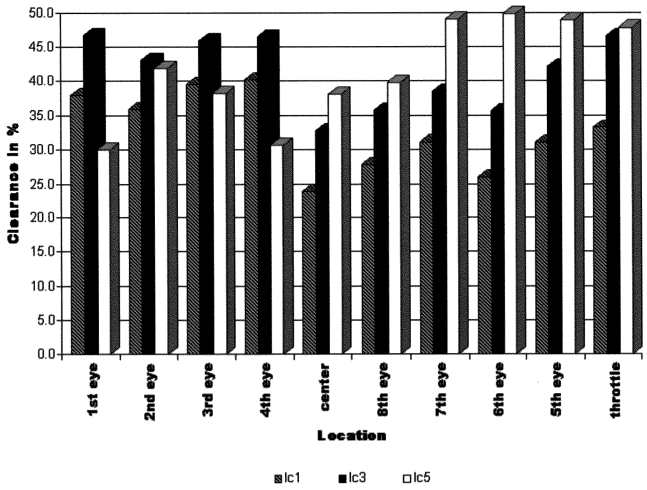

Figure 37. Remaining Clearances at Annular Seal Locations, Case Ring Bound.

Whether, in reality, the case rings are bound or not bound is difficult to answer. This depends on many factors, such as actual machine case geometry. Bore alignment, position, and distortion will also influence whether the case rings are bound or not bound to the casing.

The thermal ramp with a 20°F/min up gradient, to a maximum temperature of 400°F, is the most severe case when assuming that the case rings are bound by the pump case.

CONCLUSIONS

We believe that reasonable assumptions have been made to determine how much remaining running clearance is available at each wear ring location. Remaining clearances are above 30 percent when the case ring is not bound. When the case ring is bound, remaining clearances for three wear ring locations drop below 30 percent. The minimum clearance is 24 percent at center bush location for thermal load case 1 (20°F/min up, after 16 min and 30 sec), which results in the most severe distortion. Actual remaining clearances depend on component machine geometry, bore alignment, and actual thermal distortion. Therefore, the remaining wear ring clearances will likely be between 24 percent and 40 percent.

The use of martensitic chrome steel stationary pump wear parts was investigated in this report. Ni-resist, another common wear ring material (ASTM A436 Type 1 or 6) has a much higher thermal expansion coefficient. Therefore, its thermal growth is excessive compared with the casing. This difference in thermal expansion can cause problems during the transients investigated. Ni-resist is not recommended to be used for boiler feedpumps with the thermal transients as described in this paper.

With increased bolt loads, the gasket compression can be improved and "wetted" areas reduced. An increase of 15 percent in bolt pretension would be acceptable. Moving the bolts closer to the centerline on the discharge side can improve gasket compression even further.

The casing appears to be structurally weaker around the discharge volute top half. Improvements could be made by adding more material to the parting flange on this side, or by accommodating a stiffening rib along this side.

Additional analysis runs would be needed to clarify whether design changes to the pump or gasket material can improve the internal leakage across the volutes. The influence of higher bolt loads on the gasket compression also needs to be quantified.

Under more demanding operating conditions, the pump user can expect increased availability of the boiler feedpump, which will reduce equipment operating cost. With the use of fluid dynamics computer programs, this model can also be employed for the optimization of the hydraulic passages.

Finite element analysis is a tool that can be used to evaluate very complex geometries and physical boundary conditions. Costly testing can sometimes be avoided in determining equipment suitability for severe operating conditions. However, modelling and analyses are complex tasks, requiring both the proper tools and the user's knowledge of how to interpret and evaluate the obtained results.

REFERENCES

ABAQUS Version 5.5, Hibbit, Karlsson & Sorensen, Inc., Pawtucket, Rhode Island.

ANSYS Version 5.3, ANSYS, Inc., Canonsburg, Pennsylvania.

Unigraphics Solutions, Inc., EDS (Electronic Data Systems Corporation), Maryland Heights, Missouri.

BIBLIOGRAPHY

Deitz, D., March 1997, "The Convergence of Design and Analysis," *Mechanical Engineering*.

Eckert, E. R. G. and Drake, R. M., Jr., 1987, *Analysis of Heat and Mass Transfer*, Hemisphere, New York: Hemisphere Publishing Corporation.

"Effective Techniques for Solving Large Problems with ABAQUS," Presented at the 1997 ABAQUS Users' Conference, Milan, Italy.

Eisenberg, B., April 1996, "Is FEA Headed for Prime Time?" *Product Design and Development*.

Groth, C. and Mueller, G., "FEM fuer Praktiker—Temperaturfelder," Expert Verlag, Technische Akademie Esslingen.

Izurieta, C., Summer 1998, "CAD Model Quality Holds the Key for Analysis," *Analysis Solutions*.

Mueller, G. and Huethig, A., "Finite Element, Einfuehrung in das Arbeiten mit Ansys an nachvollziehbalren Beispielen," Verlag Heidelberg.

Riotto, J., March 1997, "Re-engineering the Workstation," *Mechanical Engineering*.

"Thermal Analysis, A Revision 5.0 Tutorial," Swanson Analysis Systems, Inc., Houston, Pennsylvania.